Optical analog of spontaneous symmetry breaking induced by tachyon condensation in amplifying plasmonic arrays

A. Marini,[1] Tr. X. Tran,[1,2] S. Roy,[1,3] S. Longhi,[4] and F. Biancalana[1,5,*]

[1]*Max Planck Institute for the Science of Light, Guenther-Scharowsky-Straße 1, 91058 Erlangen, Germany*
[2]*Department of Physics, Le Quy Don University, 236 Hoang Quoc Viet Street, 10000 Hanoi, Vietnam*
[3]*Department of Physics and Meteorology, Indian Institute of Technology, Kharagpur-721302, India*
[4]*Dipartimento di Fisica, Politecnico di Milano, and IFN-CNR, Piazza L. da Vinci 32, I-20133 Milano, Italy*
[5]*School of Engineering & Physical Sciences, Heriot-Watt University, Edinburgh, EH144AS, United Kingdom*

(Received 10 September 2013; revised manuscript received 20 January 2014; published 24 February 2014)

We study analytically and numerically an optical analog of tachyon condensation in amplifying plasmonic arrays. Optical propagation is modeled through coupled-mode equations, which in the continuous limit can be converted into a nonlinear one-dimensional Dirac-like equation for fermionic particles with imaginary mass, i.e., fermionic tachyons. We demonstrate that the vacuum state is unstable and acquires an expectation value with broken chiral symmetry, corresponding to the homogeneous nonlinear stationary solution of the system. The quantum field theory analog of this process is the condensation of unstable fermionic tachyons into massive particles. This paves the way for using amplifying plasmonic arrays as a classical laboratory for spontaneous symmetry breaking effects in quantum field theory.

DOI: 10.1103/PhysRevA.89.023840 PACS number(s): 42.65.Wi, 42.82.Et, 42.79.Gn

I. INTRODUCTION

Photonic crystals and their one-dimensional realizations—waveguide arrays (WAs)—have been extensively studied in order to mimic the nonrelativistic dynamics of quantum particles in periodic potentials [1–3]. In this respect, WAs constitute a useful classical laboratory for simulating quantum effects and can be used either to analyze well-known fundamental mechanisms such as Bloch oscillations [4], Zener tunneling [5,6], optical dynamical localization [7], and Anderson localization in disordered lattices [8], or even possibly uncover novel quantum effects. The thorough correspondence between the Schrödinger equation for the quantum wave function and the paraxial equation for the optical field is the key that makes it possible to establish a precise quantum-optical analogy. Similarly, it is possible to mimic relativistic phenomena of quantum field theories in binary waveguide arrays (BWAs), since optical propagation in the continuous limit is governed by a $(1+1)$-dimensional Dirac equation [9]. Several mechanisms such as Klein tunneling [10], Zitterbewegung [11], Klein paradox [12], and fermion pair production [13] have been observed in BWAs. Analytical soliton solutions of the discrete coupled-mode equations (CMEs) for a BWA, constituting the optical analog of the (1+1)-dimensional nonlinear relativistic Dirac equation, have been recently reported [14]. Although there is no evidence of fundamental nonlinearities in quantum field theory (QFT), the nonlinear Dirac equation has constituted a matter of study for a long time and it has been used as an effective theory in atomic [15], nuclear and gravitational physics [16] and in the study of ultracold atoms [17]. An intriguing mechanism arising in quantum field theories is represented by *tachyon condensation* [18]. This is a process in particle physics where the system lowers its energy by spontaneously generating particles. The tachyonic field with complex mass is unstable and acquires a vacuum expectation value reaching the minimum of the potential energy and getting a non-negative squared mass. This mechanism is intimately related to the process of *spontaneous symmetry breaking*, i.e., the spontaneous collapse of a system into solutions that violate one or more symmetries of the governing equation, which in other contexts is responsible for the existence of Higgs bosons [19], Nambu-Goldstone bosons [20,21], and fermions [22]. Motivated by the importance of using BWAs as a classical laboratory for the study of QFT phenomena, in this paper we theoretically investigate optical propagation in amplifying plasmonic arrays with alternate couplings, which in the continuous limit are governed by a nonlinear Dirac-like equation with imaginary mass. We find that the vacuum state is unstable and acquires an expectation value with *broken chiral symmetry* corresponding to the dissipative nonlinear stationary mode. We also study modulational instability, finding the conditions where the new vacuum is stable and unstable due to the presence of topological defects, i.e., dissipative solitons. This paves the way for using BWAs to simulate tachyon condensation and spontaneous symmetry breaking mechanisms arising in QFT.

II. MODEL

In the following we consider an amplifying plasmonic array—a layered metal-dielectric stack—sketched in Fig. 1. Surface plasmon polaritons (SPPs) propagating at every y-z metal-dielectric interface are weakly coupled to nearest neighbors through alternating positive and negative couplings [23]. This condition can also be achieved in BWAs either through a Bragg structure with a low-index defect [24] or through waveguides with propagation constants that vary periodically along the propagation direction [9,25]. Amplification schemes with SPPs have been intensively studied and also demonstrated experimentally [26,27]. Gain is provided by externally pumped active inclusions embedded in the dielectric layers that can be modeled as two-level atoms.

*Andrea.Marini@mpl.mpg.de

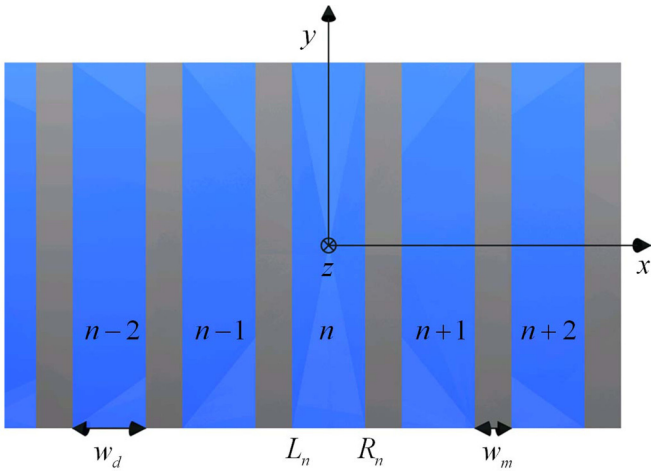

FIG. 1. (Color online) Illustrative sketch of the structure analyzed in this work: a layered metal-dielectric stack supporting SPPs at every z-y interface. The dielectric media (blue slabs) embed externally pumped active inclusions, which amplify SPPs propagating along the z direction. Every nth dielectric slab of width w_d, adjacent to a metallic stripe of thickness w_m, supports SPPs at the left and right interfaces with optical amplitudes L_n, R_n. The system is assumed homogeneous in the y,z directions and infinitely extended in the x,y,z directions.

For continuous monochromatic waves oscillating with angular frequency ω, the complex susceptibility ϵ_d of the pumped dielectric media is inherently nonlinear [28]: $\epsilon_d = \epsilon_b + \alpha(\delta - i)/(1 + \delta^2 + |\mathbf{E}/E_S|^2)$, where ϵ_b is the linear susceptibility of the hosting medium, α is the dimensionless gain rescaled to ω/c, c is the speed of light in vacuum, δ is the dimensionless detuning from resonance rescaled to the dephasing rate, E_S is the saturation field, and $\mathbf{E}$ is the electric field of the optical wave. For weak optical fields much smaller than the saturation field, the full-saturated susceptibility can be approximated by its first-order Taylor expansion in terms of $|\mathbf{E}/E_S|^2$: $\epsilon_d \simeq \epsilon_{d0} + \chi_3|\mathbf{E}|^2$, where the zeroth-order term $\epsilon_{d0} = \epsilon_b + \alpha(\delta - i)/(1 + \delta^2)$ accounts for linear susceptibility and gain, while the coefficient $\chi_3 = \alpha(i - \delta)/(E_S + \delta^2 E_S)^2$ accounts for focusing or defocusing nonlinearity (depending on the sign of the detuning δ) and nonlinear saturation of the gain.

In the limit of weak nonlinearity and overlap between adjacent SPPs (see Appendix), optical propagation in the amplifying plasmonic array sketched in Fig. 1 can be modeled by the following pair of CMEs [23]:

$$i\frac{dL_n}{dz} - i\eta L_n + \kappa(R_n - R_{n-1}) + \gamma|L_n|^2 L_n = 0, \quad (1)$$

$$i\frac{dR_n}{dz} - i\eta R_n + \kappa(L_n - L_{n+1}) + \gamma|R_n|^2 R_n = 0, \quad (2)$$

where $\eta = \eta' + i\eta''$, $\eta' > 0$ is the effective gain parameter, η'' is the linear phase shift induced by two-level atoms ($\eta'' = 0$ at resonance), κ, γ are the coupling and nonlinear coefficients, and L_n, R_n are the left and right dimensionless field amplitudes at every nth dielectric slot (see Fig. 1). The longitudinal coordinate z is normalized to the scaling length z_0, which is arbitrary and can be chosen conveniently. In what follows, we will set z_0 to be the coupling length, so that $\kappa = 1$ and η, γ are complex dimensionless constants. At $\lambda = 594$ nm, using a silver stripe of width $w_m = 45$ nm ($\epsilon_m = -12.33 + 0.97i$) and a gaining medium of width $w_d = 260$ nm and $\epsilon_d = 2.13 - 0.05i$, one gets a coupling length of $z_0 \simeq 1$ μm, and realistic values for the gain parameter are of the order $|\eta| \simeq 10^{-2}$. The full field $\mathbf{E}$ is given by the linear superposition $\mathbf{E}(x,z,t) = E_S \sum_{n=-\infty}^{+\infty}\{L_n(z)\mathbf{e}_{L,n}(x) + R_n(z)\mathbf{e}_{R,n}(x)\}e^{i\beta z - i\omega t}$, where the (dimensionless) vectors $\mathbf{e}_{L,n}(x)$ and $\mathbf{e}_{R,n}(x)$ are the unperturbed linear mode profiles and β is the propagation constant of SPPs at every metal-dielectric interface. Owing to the assumption of small overlap between adjacent SPPs, the linear unperturbed dispersion $\beta(\omega)$ coincides with the well-known single-interface dispersion (see Appendix). A full detailed derivation of Eqs. (1) and (2) and analytical expressions for the coefficients η, κ, γ are given in Refs. [23,28–30]. In the Appendix we report the rigorous derivation of Eqs. (1) and (2) starting from the full vectorial Maxwell equations and using a multiscale expansion. We emphasize that predictions of CMEs in the limit of small overlap between adjacent SPPs [23] find agreement with full vectorial calculations [31,32] and our model is fully justified.

Note that the following calculations are not dependent on the particular value of the saturation field E_S, which scales the optical field. Owing to the dual chirality of alternating metal-dielectric interfaces (metal-dielectric and dielectric-metal), the system is inherently binary and every SPP is coupled with left and right adjacent SPPs by means of two different coupling coefficients κ_L, κ_R. However, it is possible to adjust the width of the dielectric slabs (w_d) and metallic stripes (w_m) in order to achieve the condition $\kappa_L = -\kappa_R = \kappa$ [23]. The nonlinear coefficient is complex $\gamma = \gamma' + i\gamma''$, the real part can be either positive or negative depending on the sign of the detuning $\gamma' \propto \delta/(1 + \delta^2)^2$, while the imaginary part is always positive $\gamma'' > 0$ and accounts for the nonlinear saturation of gain. Note that Eqs. (1) and (2) are invariant under reflection in the x direction ($n \to -n$, $L_n \to R_{-n}$, $R_n \to L_{-n}$), due to the inherent chiral symmetry of the total system. Note that, since our model assumes an infinitely extended metal-dielectric stack, we neglect boundary effects due to finite size, which are expected to be negligible in practical samples if the number of layers is large and transversal dimensions are much greater than the optical wavelength.

A. Vacuum expectation value

Owing to the externally pumped active inclusions, small perturbations of the vacuum state $L_n = R_n = 0$ are exponentially amplified at a rate η'. Instability develops until nonlinear effects become important and nonlinear gain saturation comes into play counterbalancing the linear amplification. Homogeneous nonlinear stationary modes of Eqs. (1) and (2) can be found by taking the *Ansätze* $L_n = L_0 e^{iqn + i\mu z}$, $R_n = R_0 e^{iqn + i\mu z}$, where q is the transverse momentum and μ is the nonlinear correction to the unperturbed propagation constant β. As a consequence of the dissipative nature of the system, the amplitudes L_0, R_0 do not remain arbitrary and their moduli are fixed to be $A = \sqrt{\eta'/\gamma''}$. The nonlinear correction to the propagation constant is given by $\mu_\pm = \eta'' \pm 2k \sin(q/2) + \gamma'\eta'/\gamma''$. The amplitude of the dissipative

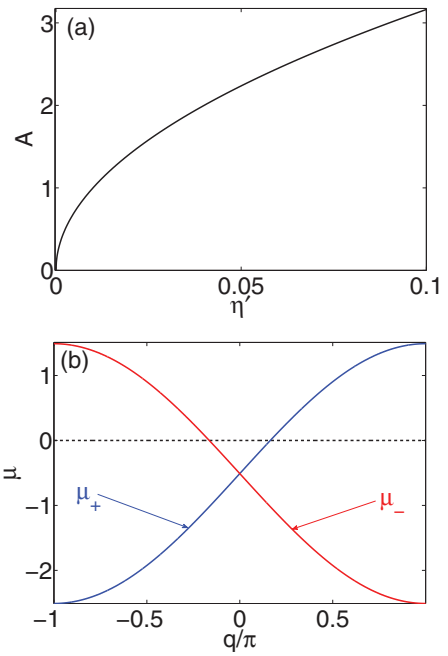

FIG. 2. (Color online) (a) Amplitude of the dissipative nonlinear mode A as a function of the effective gain η' for $\gamma'' = 0.01i$. (b) Nonlinear dispersion $\mu_{\pm}(q)$ as a function of q/π for $\eta = 0.01 - 0.5i$, $k = 1$, and $\gamma = -0.01 + 0.01i$. Blue and red curves represent the two dispersion branches μ_+, μ_-. The black dashed line denotes $\mu = 0$.

nonlinear mode A is plotted as a function of the effective gain parameter η' in Fig. 2(a), while the nonlinear dispersion $\mu_{\pm}(q)$ is depicted in Fig. 2(b). Note that, due to the inherent alternate coupling of the system, the nonlinear dispersion is characterized by a Dirac diabolical point at $q = 0$ [33]. At this special point, the phases of both amplitudes L_0, R_0 remain arbitrary. Conversely, for $q \neq 0$ the mode amplitudes are fixed to $R_0 = \mp i e^{iq/2} L_0$ and only a global phase is left arbitrary.

B. Nonlinear Dirac-like equation

As mentioned in the Introduction, BWAs have been used to mimic phenomena in both nonrelativistic and relativistic quantum mechanics [2,11], since CMEs can be converted into the one-dimensional relativistic Dirac equation [34]. Defining the two-component spinor $\psi = [L_n(z), R_n(z)]^T$, if the transversal patterns of the amplitudes L_n, R_n are smooth, one can take the continuous limit by introducing the continuous spatial coordinate $n \to x$. In this limit, the spinor satisfies the (1+1)-dimensional nonlinear Dirac-like equation

$$i\partial_z \psi - i\eta\psi + i\kappa\hat{\sigma}_y \partial_x \psi + \gamma G(\psi) = 0, \qquad (3)$$

where $G(\psi) = (|L|^2 L, |R|^2 R)^T$ is the nonlinear spinorial term and $\hat{\sigma}_y$ is the y-Pauli matrix. In what follows, we will focus on the case where the angular frequency of SPP ω coincides with the two-level atom resonant frequency and thus the detuning δ vanishes: $\delta = 0$, so that $\eta = \eta'$ and $\gamma = i\gamma''$. In this case Eq. (3) is analogous to the (1+1)-dimensional Thirring model [35] with imaginary mass and nonlinear terms, describing the dynamics of fermionic tachyons. Optical analogs of fermionic tachyons have been recently investigated in optical graphene and in topological insulators [36,37]. Note that Eq. (3) is a *Dirac-like* equation, since the "mass term" $(-i\eta\psi)$ is different from previously studied standard formulations [11,36], and is responsible for the existence of unstable tachyonlike particles. Owing to amplification, vacuum dynamically acquires a stable expectation value and the ensuing final state is the optical analog of a condensate of stable fermionic particles with non-negative squared mass. In turn, this process is commonly named *tachyon condensation*, e.g., in the context of open string field theories [38].

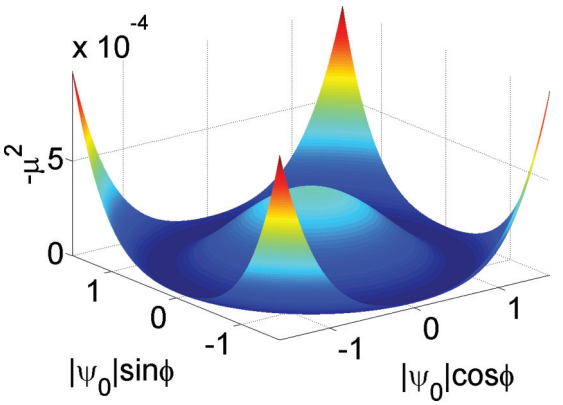

FIG. 3. (Color online) Optical analog of the sombrero potential describing spontaneous symmetry breaking in quantum field theory: $-\mu^2$ is plotted against $|\psi_0|\cos\phi$, $|\psi_0|\sin\phi$, where $|\psi_0|$ is the field amplitude and ϕ is the relative phase between the spinor components. The plot is made by taking the parameters $\eta' = 0.02$, $\kappa = 1$, $\gamma'' = 0.01i$.

III. SPONTANEOUS SYMMETRY BREAKING

Note that, analogously to the Thirring [35], sine-Gordon [39], and Nambu-Jona-Lasinio [20] models, Eq. (3) is chirally symmetric since it is left invariant under reflection $x \to -x$ if the spinor components are transformed as $L(x) \to R(-x)$, $R(x) \to L(-x)$. In turn, while the unstable vacuum state $\psi = 0$ is chirally symmetric, the nonlinear homogeneous mode $\psi = \psi_0 e^{i\mu z}$ with finite amplitude ψ_0 and propagation constant μ [where $\mu^2 = -(\eta' - \gamma''|\psi_0|^2)^2$] breaks the chiral symmetry. The optical analog of energy is represented by the propagation constant μ and the system spontaneously evolves to states where $-\mu^2$ is minimum. In Fig. 3, we plot $-\mu^2 = (\eta' - \gamma''|\psi_0|^2)^2$ as a function of the mode amplitude $|\psi_0|$ and the relative phase between the spinor components ϕ. We find the characteristic sombrero profile, which constitutes the archetypical potential describing spontaneous symmetry breaking in QFT. Our optical analog of tachyon condensation thus drives the physical system to a stable state with broken chiral symmetry where $-\mu^2$ is minimum and particles (i.e., optical states) with non-negative squared mass are generated.

IV. MODULATIONAL INSTABILITY

In order to study the stability of the nonlinear homogeneous stationary mode with broken chiral symmetry under

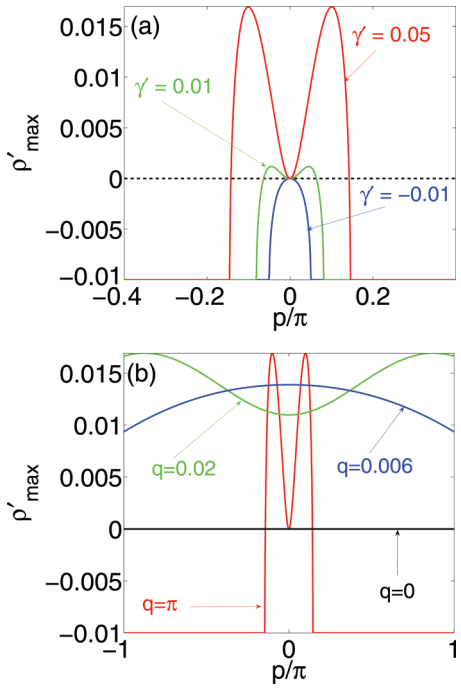

FIG. 4. (Color online) Maximum instability eigenvalue $\rho'_{\max}$ as a function of the transverse momentum p of perturbating waves. (a) $\rho'_{\max}$ vs p for $q=\pi$, $\kappa=1$, $\eta'=0.01$, $\gamma''=0.02i$, and several values of γ'. Blue, green, and red curves correspond to $\gamma'=-0.01,0.01,0.05$. The black dashed line denotes the instability threshold $\rho'_{\max}=0$. (b) $\rho'_{\max}$ vs p for $\kappa=1$, $\eta'=0.01$, $\gamma=0.05+0.02i$, and several values of q. Black, blue, green, and red curves correspond to $q=0,0.006,0.02,\pi$.

transversal modulation, we perturb it with small amplitude waves carrying transverse momentum p:

$$L_n=[L_0+l_+e^{ipn+\rho z}+l_-^*e^{-ipn+\rho^* z}]e^{iqn+i\mu z}, \quad (4)$$

$$R_n=[R_0+r_+e^{ipn+\rho z}+r_-^*e^{-ipn+\rho^* z}]e^{iqn+i\mu z}. \quad (5)$$

Inserting Eqs. (4) and (5) into Eqs. (1) and (2) and linearizing for small $|l_\pm|,|r_\pm|$ one finds a fourth-order homogeneous system of algebraic equations $[\hat{\mathcal{M}}-\rho\hat{1}]\mathbf{v}=0$, where $\mathbf{v}=(l_+,l_-,r_+,r_-)^T$, $\hat{1}$ is the identity matrix, $\hat{\mathcal{M}}$ is the linearized system matrix, and ρ_1, ρ_2, ρ_3, and ρ_4 are the instability eigenvalues of $\hat{\mathcal{M}}$ that we have calculated numerically. Instability occurs if one of the complex eigenvalues ρ has a positive real part. In Figs. 4(a) and 4(b) we plot the real part $\rho'_{\max}$ of the most unstable eigenvalue as a function of the transverse momentum p of perturbating waves for $\kappa=1$, $\eta'=0.01$, and $\gamma''=0.02i$. In Fig. 4(a), $\rho'_{\max}$ is plotted for $q=\pi$ and $\gamma'=-0.01,0.01,0.05$ (blue, green, and red curves), while in Fig. 4(b) the real part of the nonlinear coefficient is fixed to $\gamma'=0.05$ and $q=0,0.006,0.02,\pi$ (black, blue, green, and red curves). In both figures, the instability eigenvalues were calculated for the modes of the upper branch (μ_+; see Fig. 2). Note that, for $q\neq 0$, stability depends on the sign of γ' (instability for $\gamma'>0$ and stability for $\gamma'<0$) and thus on the sign of the detuning δ. Conversely, at the Dirac point $q=0$, homogeneous nonlinear waves are always marginally stable ($\rho'_{\max}=0$).

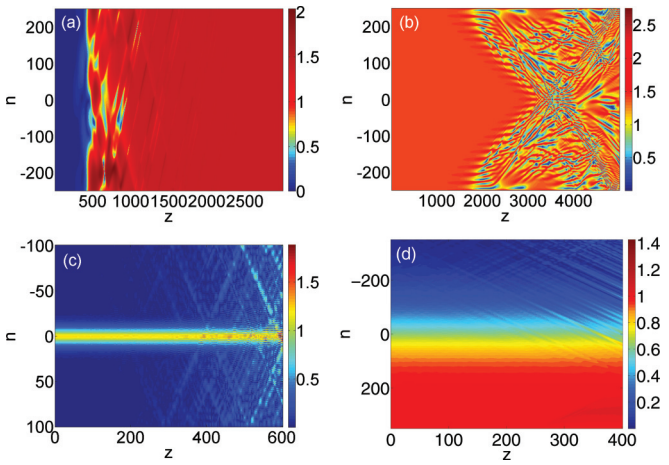

FIG. 5. (Color online) Propagation contour plots of the left field amplitude $|L_n|$ for several input conditions $L_n(0),R_n(0)$ weakly perturbed with random noise: (a) vacuum state $L_n(0)=R_n(0)=0$, (b) nonlinear homogeneous mode at the band edge $L_n(0)=R_n(0)=\sqrt{\eta'/\gamma''}e^{i\pi n}$, (c) bright soliton with $q=\pi$, and (d) kink soliton with $q=0$. Numerical integration is taken with the parameters $\eta=0.01$, $\kappa=1$ and (a) $\gamma=0.01i$ and [(b)–(d)] $\gamma=0.01+0.01i$.

These predictions have also been confirmed by the direct numerical integration of Eqs. (1) and (2) using a fourth-order Runge-Kutta algorithm. In the panels of Fig. 5, we contour plot the modulus of the left optical field $|L_n|$ as a function of the SPP index n and of the propagation direction z for different input conditions. In Fig. 5(a), we set as initial condition a small random perturbation of the vacuum state, which is unstable and dynamically converges to the stable nonlinear homogeneous mode at the Dirac point $q=0$, which represents the vacuum expectation value. In Fig. 5(b), we perturb the homogeneous nonlinear mode of the upper branch at the band edge $q=\pi$ with small random perturbations, finding a modulationally unstable chaotic dynamics. Indeed, modulational instability is strongly related to the presence of topological defects, which we have found in the present system as kink, bright, and dark dissipative solitons. Due to the instability of the vacuum background, topological defects are also unstable and behave as strange attractors for the dynamical system. We have numerically calculated the bright and kink soliton profiles by using the shooting method. In Figs. 5(c) and 5(d), we perturb bright and kink solitons with small random waves finding that the background noise is amplified and eventually destroys the solitons.

V. CONCLUSIONS

In this paper we have studied an optical analog of spontaneous symmetry breaking induced by tachyon condensation. We focused our attention on amplified SPPs propagating at every interface of a metal-dielectric stack, but our results are valid also for amplifying BWAs with alternating couplings. Optical propagation is modeled through CMEs, which in the continuous limit converge to a nonlinear Dirac-like equation that conserves chirality. We find that the vacuum is unstable and the system spontaneously evolves to a stable homogeneous state with broken chiral symmetry. This symmetry breaking is

accompanied by the formation of propagating optical modes, which correspond to particles with non-negative squared mass in the QFT-optics analogy. We studied the modulational instability of the nonlinear modes of the system, and found that at the Dirac point instability never occurs. This paves the way for using amplifying plasmonic arrays as a classical laboratory for spontaneous symmetry breaking effects in quantum field theory. We also envisage that further investigations and developments of QFT-optical analogies may be found in the context of nonlinear $\mathcal{P}T$-symmetric optical systems.

ACKNOWLEDGMENTS

A.M., S.R., F.B. (Max Planck Research Group), and T.X.T. (Max Planck Partner Group) are supported by the German Max Planck Society for the Advancement of Science (MPG).

APPENDIX

1. Derivation of coupled-mode equations for a layered metal-dielectric stack

We start our derivation from the full vectorial wave equation for the monochromatic field $\mathbf{E}e^{-i\omega t}$ with angular frequency ω:

$$\nabla \times \nabla \times \mathbf{E} = \mu_0 \omega^2 \mathbf{D}, \tag{A1}$$

where μ_0 is the vacuum magnetic permeability and the physical electric field is given by the real part $\mathrm{Re}[\mathbf{E}e^{-i\omega t}]$. In the limit where the optical field is much smaller than the saturation field $E \ll E_S$, the dielectric constant of the externally pumped media is

$$\epsilon_d \simeq \epsilon_b + \delta\epsilon_d + \chi_3 |\mathbf{E}|^2, \tag{A2}$$

where $\delta\epsilon_d = \alpha(\delta - i)/(1+\delta^2)$, $\chi_3 = \alpha(i-\delta)/(E_S + \delta^2 E_S)^2$, and the quantities involved in these expressions have been defined above. Thus, the electric displacement is given by $\mathbf{D} = \epsilon_0[(\epsilon + \Delta\epsilon)\mathbf{E} + \mathbf{N}]$, where

$$\epsilon(x) = \sum_{n=-\infty}^{+\infty} \left\{ \epsilon_b \theta\left[\frac{w_d}{2} - |x - 2nw_0|\right] + \epsilon_m' \theta\left[\frac{w_m}{2} - |x - (2n+1)w_0|\right]\right\}, \tag{A3}$$

$$\Delta\epsilon(x) = \sum_{n=-\infty}^{+\infty} \left\{ \delta\epsilon_d \theta\left[\frac{w_d}{2} - |x - 2nw_0|\right] + i\epsilon_m'' \theta\left[\frac{w_m}{2} - |x - (2n+1)w_0|\right]\right\}, \tag{A4}$$

$$\mathbf{N}(x,z) = \sum_{n=-\infty}^{+\infty} \chi_3 |\mathbf{E}|^2 \mathbf{E} \theta\left[\frac{w_d}{2} - |x - 2nw_0|\right], \tag{A5}$$

where $w_0 = (w_d + w_m)/2$, $\theta(x)$ is the Heaviside step function, and the prime and double prime suffixes indicate the real and imaginary parts. Since the structure is assumed homogeneous and infinitely extended along the y direction, ∂_y derivatives in Eq. (A1) are null and it is possible to achieve a system of differential equations for the E_x, E_z field components of plasmonic TM waves ($E_y = 0$)

$$\partial_{xz}^2 E_z - \partial_{zz}^2 E_x = \mu_0 \omega^2 D_x, \tag{A6}$$

$$\partial_{xz}^2 E_x - \partial_{xx}^2 E_z = \mu_0 \omega^2 D_z. \tag{A7}$$

The magnetic field $\mathbf{H} = H_y \hat{y}$ is determined by $\mathbf{H} = \nabla \times \mathbf{E}/(i\mu_0 c)$. In what follows we are assuming that the effects of metal losses and of the active inclusions embedded in the dielectric media are small: $|\Delta\epsilon\mathbf{E}|, |\mathbf{N}| \ll |\epsilon\mathbf{E}|$. Introducing the small dummy variable s, we make the following *Ansätze*:

$$E_x(x,z) = E_S \sum_{n=-\infty}^{+\infty} [L_n(z) e_{L,x}(x - x_{L,n}) + R_n(z) e_{R,x}(x - x_{R,n})] e^{i\beta z} + \delta E_x e^{i\beta z} + o(s^{5/2}), \tag{A8}$$

$$E_z(x,z) = E_S \sum_{n=-\infty}^{+\infty} [L_n(z) e_{L,z}(x - x_{L,n}) + R_n(z) e_{R,z}(x - x_{R,n})] e^{i\beta z} + \delta E_z e^{i\beta z} + o(s^{5/2}), \tag{A9}$$

where $x_{L,n} = -w_d/2 + 2nw_0$, $x_{R,n} = w_d/2 + 2nw_0$ are the positions of left and right interfaces, $\mathbf{e}_{L,R}$ are the unperturbed mode profiles of left and right interfaces, L_n, R_n are the left and right mode amplitudes, β is the unperturbed propagation constant, and $\delta\mathbf{E}$ is the residual field correction. For the development of the multiscale expansion we assume that

$$|L_n|, |R_n| \sim o(s^{1/2}), \tag{A10}$$

$$|\Delta\epsilon|, e^{-q_d w_d}, e^{-q_m w_m} \sim o(s), \tag{A11}$$

$$|\partial_z L_n|, |\partial_z R_n|, |\delta\mathbf{E}| \sim o(s^{3/2}), \tag{A12}$$

where $q_d^2 = \beta^2 - \epsilon_b \omega^2/c^2$, $q_m^2 = \beta^2 - \epsilon_m' \omega^2/c^2$. The left and right SPP amplitudes $L_n(z), R_n(z)$ and mode profiles $\mathbf{e}_{L,R}$ are dimensionless, while the physical dimensions are carried by the saturation field E_S. The assumption that $e^{-q_d w_d}, e^{-q_m w_m}$ are small and of the same order of $|\Delta\epsilon|$ states quantitatively the approximation of weak overlap between adjacent SPPs.

2. Linear modes and dispersion: $o(s^{1/2})$ order

At the $o(s^{1/2})$ order, left (L_n) and right (R_n) SPPs are uncoupled and Maxwell equations can be reduced to the linear system of differential equations

$$\hat{\mathcal{L}}_k \mathbf{e}_k = 0, \tag{A13}$$

where the labels $k = L, R$ correspond to left and right SPPs, $\mathbf{e}_k$ are the uncoupled linear mode profiles $\mathbf{e}_k = (e_{k,x} e_{k,z})^T$, and

$$\hat{\mathcal{L}}_k = \begin{pmatrix} \beta^2 - \epsilon_k \omega^2/c^2 & i\beta\partial_x \\ i\beta\partial_x & -\epsilon_k \omega^2/c^2 - \partial_{xx}^2 \end{pmatrix}. \tag{A14}$$

The unperturbed dielectric susceptibility profiles $\epsilon_k = \epsilon_{L,R}$ represent single isolated left and right interfaces and are

explicitly given by

$$\epsilon_L = \epsilon'_m \theta(-x + x_{L,n}) + \epsilon_b \theta(x - x_{L,n}), \tag{A15}$$

$$\epsilon_R = \epsilon'_m \theta(x - x_{R,n}) + \epsilon_b \theta(-x + x_{R,n}). \tag{A16}$$

Boundary conditions (BCs) at $o(s^{1/2})$ order require the continuity of $e_{k,z}$ and $\epsilon_k e_{k,x}$ at the interfaces $x = x_{L,n}, x_{R,n}$ ($x_{L,n}$ for $k = L$ and $x_{R,n}$ for $k = R$):

$$\epsilon_b e_{L,x}(x^+_{L,n}) = \epsilon'_m e_{L,x}(x^-_{L,n}), \tag{A17}$$

$$e_{L,z}(x^+_{L,n}) = e_{L,z}(x^-_{L,n}), \tag{A18}$$

$$\epsilon'_m e_{R,x}(x^+_{R,n}) = \epsilon_b e_{R,x}(x^+_{R,n}), \tag{A19}$$

$$e_{R,z}(x^+_{R,n}) = e_{R,z}(x^-_{R,n}). \tag{A20}$$

Equation (A13) can be solved straightforwardly, yielding the mode profiles $\mathbf{e}_{L,R}$:

$$\mathbf{e}_L(x - x_{L,n}) = \begin{pmatrix} \frac{i\beta}{q_d} \\ 1 \end{pmatrix} e^{-q_d(x - x_{L,n})} \theta(x - x_{L,n}) + \begin{pmatrix} -\frac{i\beta}{q_m} \\ 1 \end{pmatrix} e^{q_m(x - x_{L,n})} \theta(-x + x_{L,n}), \tag{A21}$$

$$\mathbf{e}_R(x - x_{R,n}) = \begin{pmatrix} \frac{i\beta}{q_m} \\ 1 \end{pmatrix} e^{-q_m(x - x_{R,n})} \theta(x - x_{R,n}) + \begin{pmatrix} -\frac{i\beta}{q_d} \\ 1 \end{pmatrix} e^{q_d(x - x_{R,n})} \theta(-x + x_{R,n}). \tag{A22}$$

Inserting Eqs. (A21) and (A22) into Eqs. (A17)–(A20), one achieves the linear dispersion law for SPPs at a single isolated interface

$$\beta = \frac{\omega}{c} \sqrt{\frac{\epsilon_b \epsilon'_m}{\epsilon_b + \epsilon'_m}}. \tag{A23}$$

Note that the unperturbed dispersion does not depend on the chirality of the system, i.e., it is the same for both left and right single isolated interfaces.

3. Solvability condition and coupled-mode equations: $o(s^{3/2})$ order

At the $o(s^{3/2})$ order, the linearized Maxwell equations for the residual field $\delta\mathbf{E} = (\delta E_x \delta E_z)^T$ yield

$$\hat{\mathcal{L}}\delta\mathbf{E} + E_S \hat{\mathcal{L}}[R_{n-1}\mathbf{e}_{R,n-1} + L_n \mathbf{e}_{L,n} + R_n \mathbf{e}_{R,n} + L_{n+1}\mathbf{e}_{L,n+1}] + E_S \hat{\mathcal{F}}[L_n \mathbf{e}_{L,n} + R_n \mathbf{e}_{R,n}] - \frac{\omega^2}{c^2} \chi_3 E_S^3 [|L_n|^2 L_n |\mathbf{e}_{L,n}|^2 \mathbf{e}_{L,n} + |R_n|^2 R_n |\mathbf{e}_{R,n}|^2 \mathbf{e}_{R,n}] = 0, \tag{A24}$$

where

$$\hat{\mathcal{F}} = \begin{pmatrix} -\Delta\epsilon\omega^2/c^2 - 2i\beta\partial_z & \partial^2_{xz} \\ \partial^2_{xz} & -\Delta\epsilon\omega^2/c^2 \end{pmatrix}. \tag{A25}$$

At the $o(s^{3/2})$ order, only contributions from nearest SPP neighbors enter the equation for the residual field $\delta\mathbf{E}$. Note that the linear operator

$$\hat{\mathcal{L}} = \begin{pmatrix} \beta^2 - \epsilon\omega^2/c^2 & i\beta\partial_x \\ i\beta\partial_x & -\epsilon\omega^2/c^2 - \partial^2_{xx} \end{pmatrix} \tag{A26}$$

does not coincide with $\hat{\mathcal{L}}_{L,R}$. Indeed, $\hat{\mathcal{L}}$ depends on the complete dielectric susceptibility profile ϵ, while $\hat{\mathcal{L}}_{L,R}$ depend on the single interface profiles $\epsilon_{L,R}$. As a result, the linear $o(s^{1/2})$ order modes $\mathbf{e}_L, \mathbf{e}_R$ are not eigenvectors of the operator $\hat{\mathcal{L}}$, which accounts for the coupling terms between adjacent SPPs. The nonlinear BCs at $o(s^{3/2})$ order are achieved from the full BCs

$$E_z(x^+_{L,n}) = E_z(x^-_{L,n}), \tag{A27}$$

$$E_z(x^+_{R,n}) = E_z(x^-_{R,n}), \tag{A28}$$

$$\epsilon_m E_x(x^-_{L,n}) = [\epsilon_b + \delta\epsilon_d] E_x(x^+_{L,n}) + N_x(x^+_{L,n}), \tag{A29}$$

$$\epsilon_m E_x(x^+_{R,n}) = [\epsilon_b + \delta\epsilon_d] E_x(x^-_{R,n}) + N_x(x^-_{R,n}), \tag{A30}$$

by retaining only $o(s^{3/2})$ terms. Following the same procedure described in Refs. [28–30], we take the scalar product of Eq. (A24) with the single interface linear modes $\mathbf{e}_L, \mathbf{e}_R$. Equations (A27)–(A30) enter the off-integral terms arising from integration by parts, which is applied to calculate the scalar products. The coupling coefficients through dielectric κ_d and metallic κ_m media ensue from the overlap integrals

$$\mathcal{O}_d = \int_{-\infty}^{+\infty} dx\, \mathbf{e}^*_L(x - x_{L,n}) \cdot \hat{\mathcal{L}} \mathbf{e}_R(x - x_{R,n}), \tag{A31}$$

$$\mathcal{O}_m = \int_{-\infty}^{+\infty} dx\, \mathbf{e}^*_R(x - x_{R,n-1}) \cdot \hat{\mathcal{L}} \mathbf{e}_L(x - x_{L,n}). \tag{A32}$$

The integral expression for the coupling coefficients κ_d, κ_m is given by

$$\kappa_d = \beta \mathcal{O}_d \left\{ 2 \int_{-\infty}^{+\infty} dx\, \epsilon(x) |e_{R,x}|^2 \right\}^{-1}, \tag{A33}$$

$$-\kappa_m = \beta \mathcal{O}_m \left\{ 2 \int_{-\infty}^{+\infty} dx\, \epsilon(x) |e_{L,x}|^2 \right\}^{-1}. \tag{A34}$$

After taking the scalar products one achieves the propagation equations for left (L_n) and right (R_n) SPP amplitudes as the solvability condition of the multiple scale expansion

$$i\frac{dL_n}{dz} = i\eta L_n - \kappa_d R_n + \kappa_m R_{n-1} - \gamma |L_n|^2 L_n, \tag{A35}$$

$$i\frac{dR_n}{dz} = i\eta R_n - \kappa_d L_n + \kappa_m L_{n+1} - \gamma |R_n|^2 R_n, \tag{A36}$$

where

$$\eta = \frac{\beta}{2(\epsilon_b + \epsilon'_m)}\left[i\frac{\epsilon'_m}{\epsilon_b}\delta\epsilon_d - \frac{\epsilon_b}{\epsilon'_m}\epsilon''_m\right], \tag{A37}$$

$$\kappa_d = \frac{2\epsilon_b\epsilon'_m\beta}{(\epsilon_b)^2 - (\epsilon'_m)^2}e^{-q_d w_d}, \tag{A38}$$

$$\kappa_m = \frac{2\epsilon_b\epsilon'_m\beta}{(\epsilon_b)^2 - (\epsilon'_m)^2}e^{-q_m w_m}, \tag{A39}$$

$$\gamma = \chi_3 E_S^2 \frac{\epsilon'_m\beta\left(q_d^2 + \beta^2\right)}{4q_d^2\epsilon_b(\epsilon_b + \epsilon'_m)}. \tag{A40}$$

The continuity of the transverse displacement D_x at every metal-dielectric interface implies a π phase jump of the transverse electric field e_x, which is discontinuous, and in turn the couplings through metallic and dielectric media have opposite signs.

[1] D. N. Christodoulides, F. Lederer, and Y. Silberberg, Nature (London) **424**, 817 (2003).
[2] S. Longhi, Laser Photonics Rev. **3**, 243 (2009).
[3] I. L. Garanovich, S. Longhi, A. A. Sukhorukov, and Y. S. Kivshar, Phys. Rep. **518**, 1 (2012).
[4] T. Pertsch, P. Dannberg, W. Elflein, A. Bräuer, and F. Lederer, Phys. Rev. Lett. **83**, 4752 (1999).
[5] M. Ghulinyan, C. J. Oton, Z. Gaburro, L. Pavesi, C. Toninelli, and D. S. Wiersma, Phys. Rev. Lett. **94**, 127401 (2005).
[6] H. Trompeter, T. Pertsch, F. Lederer, D. Michaelis, U. Streppel, A. Bräuer, and U. Peschel, Phys. Rev. Lett. **96**, 023901 (2006).
[7] S. Longhi, M. Marangoni, M. Lobino, R. Ramponi, P. Laporta, E. Cianci, and V. Foglietti, Phys. Rev. Lett. **96**, 243901 (2006).
[8] Y. Lahini, A. Avidan, F. Pozzi, M. Sorel, R. Morandotti, D. N. Christodoulides, and Y. Silberberg, Phys. Rev. Lett. **100**, 013906 (2008).
[9] J. M. Zeuner, N. K. Efremidis, R. Keil, F. Dreisow, D. N. Christodoulides, A. Tünnermann, S. Nolte, and A. Szameit, Phys. Rev. Lett. **109**, 023602 (2012).
[10] S. Longhi, Phys. Rev. B **81**, 075102 (2010).
[11] F. Dreisow, M. Heinrich, R. Keil, A. Tünnermann, S. Nolte, S. Longhi, and A. Szameit, Phys. Rev. Lett. **105**, 143902 (2010).
[12] F. Dreisow, R. Keil, A. Tünnermann, S. Nolte, S. Longhi, and A. Szameit, Europhys. Lett. **97**, 10008 (2012).
[13] S. Longhi, Appl. Phys. B **104**, 453 (2011).
[14] Tr. X. Tran, S. Longhi, and F. Biancalana, Ann. Phys. **340**, 179 (2014).
[15] D. C. Ionescu, J. Reinhardt, B. Müller, W. Greiner, and G. Soff, Phys. Rev. A **38**, 616 (1988).
[16] A. Zecca, Int. J. Theor. Phys. **41**, 421 (2002).
[17] L. H. Haddad and L. D. Carr, Europhys. Lett. **94**, 56002 (2011).
[18] G. Feinberg, Phys. Rev. **159**, 1089 (1967).
[19] P. W. Higgs, Phys. Rev. Lett. **13**, 508 (1964).
[20] Y. Nambu, Phys. Rev. **117**, 648 (1960).
[21] J. Goldstone, A. Salam, and S. Weinberg, Phys. Rev. **127**, 965 (1962).
[22] A. Salam and J. Strathdee, Phys. Lett. B **49**, 465 (1974).
[23] A. Marini, A. V. Gorbach, and D. V. Skryabin, Opt. Lett. **35**, 3532 (2010).
[24] N. K. Efremidis, P. Zhang, Z. Chen, D. N. Christodoulides, C. E. Rüter, and D. Kip, Phys. Rev. A **81**, 053817 (2010).
[25] A. Szameit, Y. V. Kartashov, F. Dreisow, M. Heinrich, T. Pertsch, S. Nolte, A. Tünnermann, V. A. Vysloukh, F. Lederer, and L. Torner, Phys. Rev. Lett. **102**, 153901 (2009).
[26] A. Marini, A. V. Gorbach, D. V. Skryabin, and A. Zayats, Opt. Lett. **34**, 2864 (2009).
[27] P. Berini and I. De Leon, Nat. Photonics **6**, 16 (2011).
[28] A. Marini and D. V. Skryabin, Phys. Rev. A **81**, 033850 (2010).
[29] D. V. Skryabin, A. V. Gorbach, and A. Marini, J. Opt. Soc. Am. B **28**, 109 (2011).
[30] A. A. Sukhorukov, A. S. Solntsev, S. S. Kruk, D. N. Neshev, and Y. S. Kivshar, Opt. Lett. **39**, 462 (2014).
[31] Y. Liu, G. Bartal, D. A. Genov, and X. Zhang, Phys. Rev. Lett. **99**, 153901 (2007).
[32] J. R. Salgueiro and Y. S. Kivshar, Appl. Phys. Lett. **97**, 081106 (2010).
[33] S. H. Nam, A. J. Taylor, and A. Efimov, Opt. Express **18**, 10120 (2010).
[34] It is important to note that, although the linear Dirac equation is Lorentz invariant, its *nonlinear* version in general is not. However, here this issue is not a concern, since in the paraxial approximation Lorentz invariance is not a requirement for a physically meaningful model.
[35] W. E. Thirring, Ann. Phys. **3**, 91 (1958).
[36] A. Szameit, M. C. Rechtsman, O. Bahat-Treidel, and M. Segev, Phys. Rev. A **84**, 021806(R) (2011).
[37] V. M. Apalkov and T. Chakraborty, Europhys. Lett. **100**, 17002 (2012).
[38] S. Hellerman and M. Schnabl, J. High Energy Phys. 04 (2013) 005.
[39] S. Coleman, Ann. Phys. **101**, 239 (1976).